

Bosonic quantum error correction with microwave cavities for quantum repeaters

S. Siddardha Chelluri,^{1,*} Sanchar Sharma,² Frank Schmidt,¹ Silvia Viola Kusminskiy,^{3,4} and Peter van Loock^{1,†}

¹*Institute of Physics, Johannes-Gutenberg University of Mainz, Staudingerweg 7, 55128 Mainz, Germany*

²*Laboratoire de Physique de l'École Normale Supérieure, ENS, Université PSL,*

CNRS, Sorbonne Université, Université de Paris, F-75005 Paris, France

³*Institute for Theoretical Solid State Physics, RWTH Aachen University, 52074 Aachen, Germany*

⁴*Max Planck Institute for the Science of Light, Staudtstraße 2, 91058 Erlangen, Germany*

(Dated: March 28, 2025)

Long-distance quantum communication necessitates the use of quantum repeaters, which typically include highly coherent quantum memories. We provide a theoretical analysis of the secret key rates for a quantum repeater system incorporating bosonic error correction and memory components. Specifically, we focus on the application of Binomial codes for two repeater segments. Using these codes, our investigation aims to suppress memory loss errors that commonly affect systems such as atoms and microwave cavities, in contrast to dephasing errors in single-spin memories. We further discuss a physical implementation of such a quantum repeater comprising a microwave cavity and a superconducting transmon, capable of state engineering with high fidelities ($> 97\%$) and logical Bell state measurements for successful entanglement swapping. As an alternative approach, we also discuss a realization in the all-optical domain.

I. INTRODUCTION

The distribution of entanglement over long distances and between multiple parties, forming quantum networks, enables numerous applications such as the quantum Internet [1], uncompromised secure communication through the establishment of private keys [2, 3], distributed quantum computing [4] and blind quantum computing [5]. However, the fiber channel transmittivity η decreases exponentially with distance between parties, making long-distance quantum communication infeasible. This limitation can be addressed by the use of quantum repeaters [6] in which a channel is divided into multiple, say n , segments. With the addition of quantum memories, this division effectively increases the channel attenuation length by a factor of n , thus enhancing the transmittivity to $\eta' = \eta^{1/n}$.

Quantum repeaters are typically classified into three generations based on their physical implementations [7]: the first relies on memories and entanglement distillation, the second on memories and error correction, and the third exclusively on error correction. As memories are crucial for the first two generations, various experimental platforms were explored as implementations, such as atomic ensembles [8], color centers in diamonds [9, 10], and quantum dots [11]. Due to decoherence in the memories, building quantum repeaters remains a significant challenge. Depending on the platform, either dephasing or loss dominates the decoherence. In the latter case, since the primary imperfection in the entire repeater system is excitation loss — both in the optical channel and the memory node — it is crucial to investigate the impact of memory loss [12]. While dephasing

in memories has been extensively studied [13–19], the loss of excitations in memories, particularly in the context of repeaters, has received relatively less attention, although prominent quantum repeater proposals would rely on memory systems subject to this type of error [8, 20]. To address loss errors, bosonic quantum error correction (QEC) can be applied, with examples including Binomial codes [21], Cat codes [22, 23], and Gottesman-Kitaev-Preskill (GKP) codes [24]. Clearly, bosonic QEC is then also applicable to those repeater systems based upon bosonic memories [25].

In this work, we present a comprehensive analysis of a two-segment, second-generation repeater with loss errors where the information is encoded as a Binomial code in the memory. In these repeaters, photons remain unencoded during transmission, allowing for repeater stations to be spaced further apart than in typical third-generation systems. Two error correction schemes are studied: one where error correction is applied once, and another where it is applied multiple times. Our figure of merit will be the secret key rate of quantum key distribution, which we numerically calculate for our repeater protocols.

A promising implementation of this quantum repeater is provided by a circuit or cavity quantum electrodynamics (cQED) setups [26, 27], consisting of a microwave circuit or a cavity coupled to a superconducting transmon. cQED setups are interesting because of the long lifetimes of the cavity photons [28], required for hosting bosonic codes, and a nearly universal control of the microwaves [29], due to the highly non-linear nature of the accompanying transmon. Note that a similar approach has been considered for a cavity using atom-light interactions [30], with a focus on Cat codes in a third-generation quantum repeater. Here, we concentrate on transmon-enabled operations that have been used experimentally to demonstrate Binomial [31], Cat [32] and GKP [33] codes. Among the rotation-invariant bosonic codes, the

* schellur@uni-mainz.de

† loock@uni-mainz.de

orthogonality of the codewords in the Binomial code is beneficial [34]. Therefore, in this work, we focus on the Binomial code.

The structure of this article is as follows: In Sec. II, we concentrate on implementing QEC with Binomial codes for a second-generation quantum repeater protocol, and calculate the corresponding secret key rates. Section III introduces a deterministic algorithm for designing Binomial codeword states, syndrome detection, and logical Bell measurements for entanglement swapping in a microwave cavity system. Additionally, in Sec. IV, we propose a protocol for logical-level entanglement swapping, achieving 50% efficiency with linear optics. All numerical simulations and results are presented in Sec. V.

II. QUANTUM REPEATERS WITH QEC FOR LOSSY MEMORIES

A quantum repeater involves dividing the channel between the communicating parties into small segments, distributing entanglement in those segments, and then using entanglement swapping to distribute the entanglement across all segments. For the rest of the paper, we consider a two-segment repeater, as illustrated in Fig. 1, with a repeater node positioned in between (i.e., memory units 2 and 3 are located close to each other). The objective is to reliably distribute Bell pairs between memory units 1 and 4 (Fig. 1).

In the first step, entanglement is independently distributed in the two segments, namely 1-2 and 3-4 (Fig. 1 (a),(b)). Given that entanglement distribution is a probabilistic process (for example, the typical success probability at 100 km is 0.01 for $L_{att} = 22$ km), multiple rounds of attempts are necessary. The time taken for each attempt is primarily given by the classical communication time $T_0 = L_0/c$, where L_0 is the repeater segment length, and c is the speed of light in optical fiber. Once a segment succeeds in generating entanglement, the corresponding qubits are stored in their respective memories. In case of failure, the memories are reinitialized and another attempt is made. This process continues until both segments achieve success.

The second step is entanglement swapping between memory units 2 and 3 (Fig. 1(c)). Entanglement swapping requires a joint Bell state measurement of one half from each of two separately entangled pairs (2 from 1-2 pair and 3 from 3-4 pair), resulting in entanglement between the remaining two halves in the respective pairs (1 and 4, Fig. 1(d))[35, 36].

Since the success of entanglement generation in each segment is independent of the other segment, we define two geometrically distributed random variables: n_{12} for segment 1-2 and n_{34} for segment 3-4. These random variables represent the number of attempts required to distribute entanglement in each segment. As the generation of entanglement is probabilistic, let us assume that segment 1-2 establishes entanglement earlier than segment

3-4. As a consequence, memory unit 2 will be waiting to swap. In general, with either memory unit 2 or 3 waiting, the waiting time is defined as $n_{diff} = |n_{12} - n_{34}|$ which follows a probability distribution p_{diff} . During this waiting period, either memory units 1 and 2 or 3 and 4 experience dissipation, leading to an exponential decrease in the swapping probability [37].

To mitigate memory loss, we encode the memory qubit using a Binomial code (see Eqs. (6), (7)) during the waiting period, thereby effectively enhancing the coherence time of the waiting memory units. The key performance metric for evaluating a quantum repeater is the (asymptotic) secret key rate, defined as

$$S = r \times R. \quad (1)$$

Here, R is the raw rate, i.e., the total number of bits transmitted per second. The fraction of the secret bits to the total bits transmitted is called secret key fraction and, considering the BB84 protocol, is given by

$$r = 1 - h(\langle e_x \rangle) - h(\langle e_z \rangle), \quad (2)$$

where the average is calculated by weighing it with the probability distribution function p_{diff} on condition that swapping is successful. Here $h(p)$ is the binary entropy function

$$h(p) = -p \log p - (1-p) \log(1-p), \quad (3)$$

and the quantum bit error rates (QBERs) e_x and e_z are defined as

$$e_z = \langle 00 | \rho_{14} | 00 \rangle + \langle 11 | \rho_{14} | 11 \rangle, \quad (4)$$

and

$$e_x = \langle +- | \rho_{14} | +- \rangle + \langle -+ | \rho_{14} | -+ \rangle. \quad (5)$$

where ρ_{14} is the density matrix of the state between memory units 1 and 4 (Fig. 1). To this end, we compare S between cases with and without encoding to assess the impact of error correction on the memories.

A. Binomial code

The Binomial code [21] is one of the bosonic codes to combat loss errors. The codewords of the lowest-order Binomial code (LBC), in the Fock basis, are

$$|\bar{0}\rangle = \frac{|0\rangle + |4\rangle}{\sqrt{2}}, \quad |\bar{1}\rangle = |2\rangle. \quad (6)$$

This corrects single-excitation loss in the bosonic memories. The next, higher-order codewords (HBC) are

$$|\bar{0}\rangle_h = \frac{|0\rangle + \sqrt{3}|6\rangle}{2}, \quad |\bar{1}\rangle_h = \frac{\sqrt{3}|3\rangle + |9\rangle}{2}. \quad (7)$$

This corrects for up to two excitation losses. We show the calculation of S explicitly for the lowest order. We then numerically simulate both codes for a two-segment repeater and compare their secret key rates S .

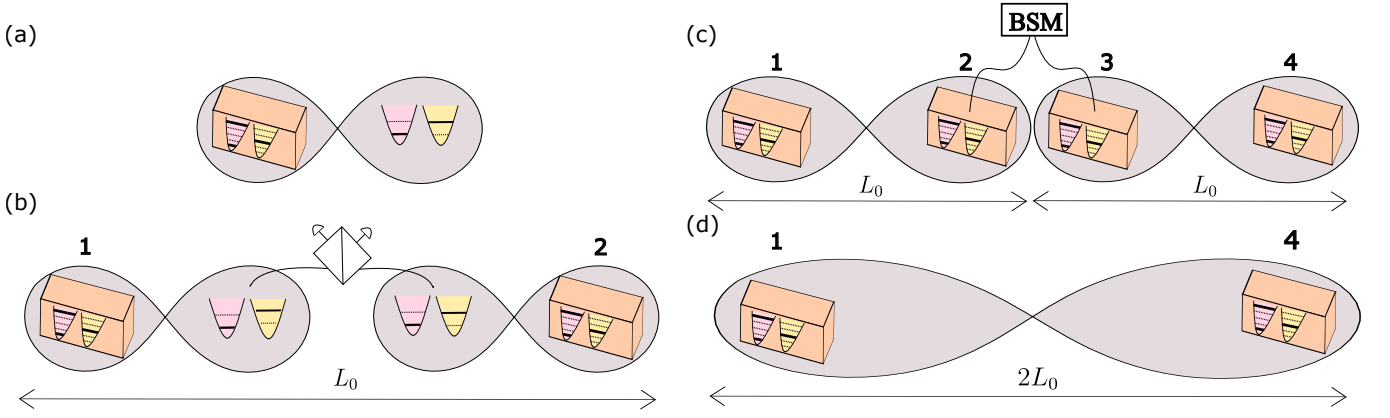


FIG. 1. Two-segment, second-generation quantum repeater, with memory implemented as a microwave cavity (shown as an example). (a) Entanglement between a travelling photon and a microwave cavity occurs at all four memory units. (b) Entanglement within a single repeater segment of distance L_0 is established between two memory units via projection measurement on travelling photons, which are conducted independently in both repeater segments. (c) Entanglement swapping occurs locally between two memory units at the middle station of the two segments via a logical Bell state measurement (BSM). (d) The final entangled state is achieved between distant memory units 1 and 4. Throughout these steps, the superposition states of the photon are represented by yellow and pink photons, though only one entangled pair of photons is distributed per round of the protocol. Cuboids represent microwave cavities, and the encoded states of the photon are depicted by the thick lines in the harmonic oscillator.

B. Secret key rate of a repeater with LBC

In this section, we discuss the calculation of the secret key rate when the memory units are encoded with LBC.

First, we generate one of the Bell states between the memory units 1-2 and 3-4. For any two memory units $\{i, j\}$, it is given by

$$|\psi^+\rangle_{ij} = \frac{|0\rangle_i |1\rangle_j + |1\rangle_i |0\rangle_j}{\sqrt{2}}. \quad (8)$$

The encoded Bell states are defined as $|\overline{\psi}^+\rangle$ by a similar definition as above with the replacements $|0, 1\rangle \rightarrow |\overline{0}, \overline{1}\rangle$. We also define the corresponding density matrix $\overline{\rho}_{ij} = |\overline{\psi}^+\rangle_{ij} \langle \overline{\psi}^+|_{ij}$.

Without loss of generality, we assume that the Bell state was successfully generated in memory units 1-2 first. While waiting for memory units 3-4, memory units 1-2 undergo amplitude damping given by the set of Kraus operators [38], E_k for all $k \in \mathbb{N}$,

$$E_k = \sum_n \sqrt{\binom{n}{k}} \sqrt{(1-\gamma)^{n-k} \gamma^k} |n-k\rangle \langle n|, \quad (9)$$

where n is the number of excitations, k is the number of excitations lost, and γ is the probability of losing an excitation stored in the memory unit.

The state of the memory units 1 and 2 after being subject to the amplitude damping channel is

$$\overline{\rho}_{12}^{dec} = \sum_{k_1, k_2=0}^4 E_{k_1,1} E_{k_2,2} \overline{\rho}_{12} E_{k_1,1}^\dagger E_{k_2,2}^\dagger, \quad (10)$$

where $E_{k,j}$ denotes k losses in mode j .

To mitigate the effect of dissipation, error correction on the encoded qubits should be performed before entanglement swapping. Syndrome detection can be done by a parity measurement as discussed in Sec. III. The recovery operation to be performed depends on the syndrome outcome. If there were no losses, the recovery operation to be performed, up to linear order of γ , is

$$\mathcal{R}_0 = |\overline{0}\rangle \langle \overline{0}^*| + |\overline{1}\rangle \langle \overline{1}^*|, \quad (11)$$

where $|\overline{0}^*\rangle = |0\rangle + (1-\gamma)^2 |4\rangle / \sqrt{2(1-2\gamma)}$ and $|\overline{1}^*\rangle = (1-\gamma) |2\rangle / \sqrt{(1-2\gamma)}$. Note that $\mathcal{R}_0 = \text{id}$ when $\gamma = 0$. If a single loss was found, the recovery operation is

$$\mathcal{R}_1 = |\overline{0}\rangle \langle 3| + |\overline{1}\rangle \langle 1|. \quad (12)$$

In \mathcal{R}_0 , the lack of complete orthogonality between error words and codewords is the cause of the significant disparity in expressions between \mathcal{R}_0 and \mathcal{R}_1 .

The next step is to perform entanglement swapping, which is achieved by projecting the joint state of memory units 2 and 3 onto the Bell basis. For example,

$$\overline{\rho}_{14} = \frac{{}_{23} \langle \overline{\psi}^+ | \overline{\rho}_{1234} | \overline{\psi}^+ \rangle_{23}}{\text{Tr} [{}_{23} \langle \overline{\psi}^+ | \overline{\rho}_{1234} | \overline{\psi}^+ \rangle_{23}]}, \quad (13)$$

with similar expressions for the other Bell states. Here, $\overline{\rho}_{1234}$ is given by $\mathcal{R}^{\otimes 2}(\overline{\rho}_{12}^{dec}) \otimes \overline{\rho}_{34}$ and \mathcal{R} is \mathcal{R}_0 or \mathcal{R}_1 depending on the error syndrome information.

The raw rate for the case of two segments with memory decay is given by [37]

$$R = \frac{\langle P_s \rangle}{\langle n_{max} \rangle T_0}, \quad (14)$$

where n_{max} is the maximum of n_{12} and n_{34} and where P_s is the swapping probability corresponding to the sum of the traces of the conditional states of the Bell measurement (the denominator in Eq. (13)) for all four Bell measurement results. The average of P_s has to be taken, because the extent to which the state $\bar{\rho}_{1234}$ is subject to memory loss depends on the random memory storage (waiting) time n_{diff} . However, we will make a distinction between the cases where the loss error correction is only performed once at the end after storage and where it is done repeatedly for multiple times at a frequency given by the elementary time unit T_0 . Both cases are treated numerically by our simulation.

The figure of merit S is calculated from R and r (defined in Eqs. (14) and (2), respectively). The secret key rates for different regimes of γ are compared for the cases of encoded and unencoded memories in Sec. V.

III. QUANTUM REPEATER WITH MICROWAVE CAVITIES

In this section, we discuss a physical implementation of the quantum repeater, introduced in Sec. II, using cQED setups. As discussed in Fig. 1, there are two microwave (MW) cavities, say A_1 and A_2 , placed at every local station, each of which are loaded with a transmon qubit $Q_{1,2}$. The first step is the generation of an entangled MW-qubit state, using local operations as discussed below. Subsequently, the state of the transmon qubit is transferred to a photon which is sent to the middle station as shown in Fig. 1. Remote entanglement swapping is performed via a joint Bell-state measurement BSM on A_1 and A_2 in the binomial-encoded basis. We discuss below a scheme for BSM using a third transmon, Q_3 , coupled to both the MW cavities.

A. Hamiltonian

The Hamiltonian for each cavity is that of a bosonic mode $H_i^a = \hbar\omega_{a,i}a_i^\dagger a_i$ for $i \in \{1, 2\}$, where $\omega_{a,i}$ and a_i are, respectively, the resonance frequency and the annihilation operator of A_i . For simplicity, we consider the resonant case $\omega_{a,1} = \omega_{a,2} = \omega_a$.

Each of the transmons are anharmonic oscillators, modelled by the Hamiltonian

$$\frac{H_i^{qs}}{\hbar} = \omega_{q,i}q_i^\dagger q_i - \frac{\alpha_i}{2}q_i^\dagger q_i \left(q_i^\dagger q_i - 1 \right), \quad (15)$$

for $i \in \{1, 2, 3\}$ where $\omega_{q,i}$, α_i , and q_i are the resonance frequency, anharmonicity, and the annihilation operator of Q_i . Furthermore, each transmon can be externally controlled via the dynamic Hamiltonian

$$\frac{H_i^{qd}(t)}{\hbar} = \Delta_i(t)q_i^\dagger q_i + \varepsilon_i(t)q_i^\dagger + \varepsilon_i^*(t)q_i, \quad (16)$$

where $\Delta_i(t)$ is the externally controllable detuning and $\varepsilon_i(t)$ is the excitation amplitude corresponding to Q_i . We assume that the cavities and transmons are so far detuned that the coupling is negligible for no external detuning, i.e. $\Delta_i = 0$. Changing the detuning Δ_i can bring Q_i in resonance with one or both of the MW cavities, allowing for entangling operations.

The individual MW-qubit couplings are in the form of a beam-splitter Hamiltonian $H_i^{aq} = \hbar g_{aq,i}(q_i^\dagger a_i + q_i a_i^\dagger)$ for $i \in \{1, 2\}$ with coupling coefficients $g_{aq,i}$. The third transmon used for BSM is coupled to both MW cavities with an effective dispersive coupling χ , modelled with

$$H^{\text{disp}} = \hbar\chi(t)q_3^\dagger q_3 \left(a_1^\dagger a_1 + a_2^\dagger a_2 \right). \quad (17)$$

The parameter χ can be tuned via the detuning Δ_3 [26, 27].

B. Entanglement generation

We want to create an entangled microwave and optical photon pair, as discussed in Fig. 1. In the first step, we create an entangled state in each MW+transmon subsystem. In this simulation, we can focus on only one MW+transmon pair ignoring the other, so we suppress the index, e.g. $a_i \rightarrow a$ and $q_i \rightarrow q$. Dissipation is added in standard Lindblad forms [39] of cavity loss, transmon loss, and transmon dephasing with corresponding Lindblad operators being a , q , and $q^\dagger q$ respectively. We consider nominal values for a cavity with $\omega_a = 2\pi \times 6$ GHz, and lifetime of 50 μs . We consider a transmon with $\omega_q = 2\pi \times 5$ GHz, $\alpha = 2\pi \times 300$ MHz, lifetime $T_1 = 10$ μs and total dephasing time $T_2^* = 5$ μs . We assume a coupling rate of $g = 2\pi \times 25$ MHz, which is sufficiently small to ensure that there is negligible MW-transmon coupling in equilibrium as $g \ll \omega_a - \omega_q$. The coupling is then induced by an input of $\Delta(t)$ that brings the MW and transmon in resonance. Complementarily, excitations in the MW+transmon subsystem are generated by exciting the transmon with the pulse $\varepsilon(t)$, as written above.

We adapt the code given in Ref. [40], to find $\Delta(t)$ and $\varepsilon(t)$ that leads to the entangled state

$$|\psi\rangle = |\bar{0}\rangle |e\rangle + |\bar{1}\rangle |g\rangle, \quad (18)$$

where MW state is encoded. Our simulations show that this state can be generated with $> 97\%$ fidelity. The fidelity is primarily limited by cavity dissipation, and thus is significantly higher for cavities with higher lifetimes. The resonance frequencies have only a weak effect on the fidelity.

The state of the transmon can be swapped into a travelling photon via a microwave-to-optical converter, creating an entangled state between microwaves and photons. While such converters are not yet realizable, there has been a significant progress in achieving partial entanglement between microwaves and optics [41–43]. Due to such a conversion being coveted for several applications, we expect such converters to be available in the future.

C. Joint Bell-state measurement

Here, we discuss how to perform a joint BSM on the two MW cavities, A_1 and A_2 , using the transmon Q_3 coupled to both of them as discussed above. In the following, we ignore the first two transmons as they are expected to stay in the ground state.

A BSM results in a 2-bit output, where each of the four possibilities correspond to the four joint MW Bell states, namely

$$\begin{aligned} |\bar{\Phi}^\pm\rangle &= \frac{|\bar{0}\bar{0}\rangle \pm |\bar{1}\bar{1}\rangle}{\sqrt{2}} \\ |\bar{\Psi}^\pm\rangle &= \frac{|\bar{0}\bar{1}\rangle \pm |\bar{1}\bar{0}\rangle}{\sqrt{2}} \end{aligned} \quad (19)$$

The state $|\bar{i}\bar{j}\rangle$ refers to the first cavity being in the i th logical state and the second cavity in the j th state. If an error has occurred on any of the cavities, their states will instead be $|\bar{0}^*\rangle$ or $|\bar{1}^*\rangle$.

First, a parity check [44] is performed on each of the cavities to find if an error has occurred. If no error has occurred, then a general state in the logical subspace is

$$|\psi\rangle_{a_1 a_2 q_3} = \sum_{ij} \alpha_{ij} |\bar{i}\bar{j}\rangle |g\rangle, \quad (20)$$

where $i, j \in \{0, 1\}$.

To separate the Ψ Bell states from the Φ Bell states, we employ the following steps. First, we apply a Hadamard gate to the qubit Q_3 by choosing $\varepsilon_3(t) = -i\varepsilon(t)$ (in rotating frame) satisfying

$$\int dt \varepsilon(t) = \frac{\pi}{4}, \quad (21)$$

to create an initial qubit state $\propto |g\rangle + |e\rangle$. Next, the dispersive coupling is turned on by reducing the detuning Δ_3 such that $\chi(t) = \chi_0$ for a time period of $t = \pi/(2\chi_0)$, and zero outside the time window. The effect of this coupling is to apply the entangling unitary on the joint system,

$$U = \exp\left[i\frac{\pi}{2} (a_1^\dagger a_1 + a_2^\dagger a_2) |e\rangle\langle e|\right]. \quad (22)$$

This unitary applies a phase on the qubit, depending on the total number of microwave photons in both cavities. The phase is periodic with photon number 4. After the two operations, the joint state of the two cavities and Q_3 becomes

$$\sum_{ij} \alpha_{ij} |\bar{i}\bar{j}\rangle \frac{|g\rangle + (-1)^{i+j} |e\rangle}{\sqrt{2}}. \quad (23)$$

Third, we apply another Hadamard gate on the transmon to get the state

$$|g\rangle (\alpha_{00} |\bar{0}\bar{0}\rangle + \alpha_{11} |\bar{1}\bar{1}\rangle) + |e\rangle (\alpha_{01} |\bar{0}\bar{1}\rangle + \alpha_{10} |\bar{1}\bar{0}\rangle).$$

Now, we can measure the qubit to separate the Ψ -states from the Φ -states. The two measurement outcomes can be written in the Bell basis as

$$|g\rangle (A_+ |\Phi^+\rangle + A_- |\Phi^-\rangle), |e\rangle (B_+ |\Psi^+\rangle + B_- |\Psi^-\rangle)$$

for coefficients A_\pm and B_\pm that can be found in terms of α -coefficients.

On the binomial code, universal gate operations were demonstrated [31]. So, we can apply a Hadamard gate on the encoded qubits in both microwave cavities to get the two possibilities depending on the outcome of the above measurement,

$$|g\rangle (A_+ |\Phi^+\rangle + A_- |\Psi^+\rangle), |e\rangle (B_+ |\Phi^-\rangle - B_- |\Psi^-\rangle).$$

We can again apply the above three steps to separate Ψ^\pm from Φ^\pm , finishing the Bell state measurement.

If an error has occurred on the first cavity, Eq. (23) will be modified as

$$\sum_{ij} \alpha_{ij} |\bar{i}^*\bar{j}\rangle \frac{|g\rangle - i(-1)^{i+j} |e\rangle}{\sqrt{2}}. \quad (24)$$

Then, we can apply a Hadamard gate preceded by a phase gate to cancel off the factor $-i$. Note that both the gates can be applied in one step by choosing $\varepsilon_3(t) = -\varepsilon(t)$ with the condition in Eq. (21). Then, the rest of the process follows in the same way.

Similarly, if an error occurred on both cavities, Eq. (23) will be modified as

$$\sum_{ij} \alpha_{ij} |\bar{i}^*\bar{j}^*\rangle \frac{|g\rangle - (-1)^{i+j} |e\rangle}{\sqrt{2}}, \quad (25)$$

and the same procedure as in the no-error case can be applied.

IV. QUANTUM REPEATER WITH QEC IN THE OPTICAL DOMAIN

Another feasible experimental platform for quantum repeaters is optics. In an all-optical approach, we could bypass the need for a microwave-to-optical conversion. However, in this case, we need to store phase-sensitive photonic states in an optical cavity system. To a certain extent, this has been experimentally demonstrated already, at least for phase-sensitive states up to one photonic excitation [45–47]. Another benefit of this all-optical approach would be that the local state processing at each repeater node can be done much faster than with light-matter interactions. The hardest element in an all-optical domain is the state preparation. There are a few experimental demonstrations of generating higher Fock states [48, 49] which are crucial to generate Binomial codeword states. Concerning the logical Bell measurements, we demonstrate that entanglement swapping can be achieved using linear optics with a 50% success rate, provided that a recovery operation is performed before the swapping process. The proof is given in the App. A.

V. SIMULATION OF SECRET KEY RATES

Here, we discuss the simulation and numerical evaluation of secret key rates for both cases, unencoded and encoded (LBC and HBC). In essence, we need to calculate Eq. (1). However, there are two possibilities in the calculation process: implementing error correction only once, referred to as single-time error correction (SEC), or implementing error correction multiple times at regular intervals during the waiting time, referred to as multiple-time error corrections (MEC). The procedure to simulate the secret key rates S with SEC is described in Sec. II. Since it is SEC, \mathcal{R} is applied only once. To numerically calculate the averages in Eq. (14), a cutoff time on the memories (apart from the exponential decay) was implemented. The swapping probability P_s is given by expressions such as the denominator of Eq. (13). For the SEC case, the cutoff was selected based on the time step corresponding to $\gamma = 0.5$. The theoretical analysis for MEC is described in App. C. In the case of MEC, $\gamma = 0.1$ with 100 as an upper limit for the maximum number of times the recovery can be performed is considered. The parameters $L_{att} = 22$ km, $c = 2 \times 10^8$ m s $^{-1}$ were used throughout. The secret key rates in both cases are calculated under the assumption of 100% efficiency in the BSM during swapping. Three different coherence times are considered for the simulations, including realistic values from state-of-the-art experiments [28] and possible future values. All simulations were performed in Mathematica.

In Fig. 2, we show the secret key rate as a function of the segment length, L_0 (range 10-200 km), assuming a highly efficient memory interface, $\eta_m = 0.95$. We observe a clear improvement in the secret key rates of the encoded schemes in comparison with the unencoded one for all three different coherence times considered. For a more imperfect memory interface, $\eta_m = 0.9$, the results are shown in Fig. 3. They exhibit a similar trend but the unencoded case gives no positive secret key rates. Interestingly, memories with error correction outperform the unencoded memories even with coherence times one order of magnitude higher.

In Fig. 4, we show the secret key fraction (r) as a function of the segment length L_0 for LBC showing the difference between the cases of SEC and MEC. As expected, allowing for multiple error corrections increases r for long distances. For sufficiently short distances, a single recovery step is more appropriate. With increasing coherence times the distance at which SEC and MEC start to deviate is also increasing. Even though the value of r is almost unity for the blue curves ($\tau_{coh} = 1$ s) at 100 km for both SEC and MEC, from Fig. 2 it is clear that the secret key rates decrease by two orders of magnitude from the initial value due to the decrease in the raw rate (R).

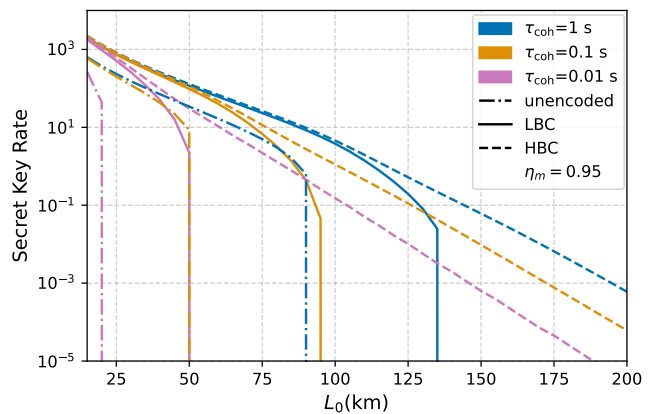


FIG. 2. Comparison of secret key rates with different memory coherence times for unencoded, Lower Binomial Code (LBC) and Higher Binomial code (HBC) when SEC is performed. The memory interface parameter $\eta_m = 0.95$.

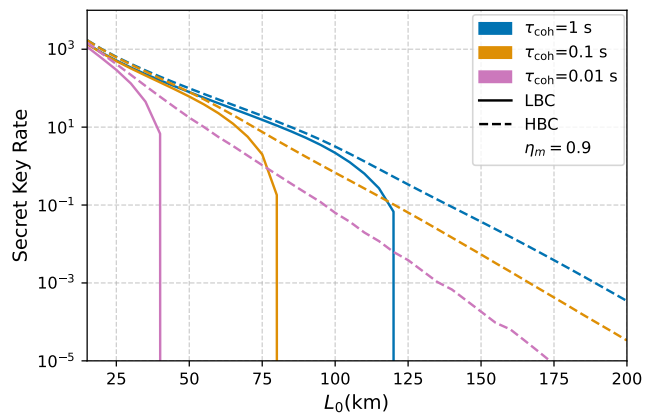


FIG. 3. Comparison of secret key rates with different memory coherence times for Lower Binomial Code (LBC) and Higher Binomial code (HBC) when SEC is performed. The memory interface parameter $\eta_m = 0.9$.

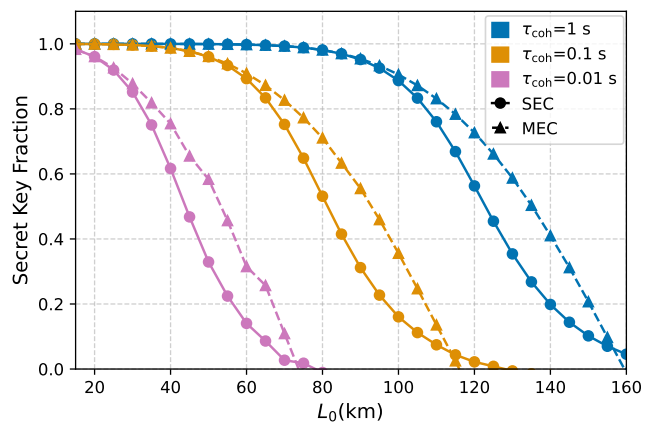


FIG. 4. Comparison of the secret key fraction of LBC with different coherence times for the cases of SEC and MEC. The memory interface parameter $\eta_m = 1.0$.

VI. CONCLUSION AND OUTLOOK

We have studied the near-term performance of a second-generation quantum repeater protocol under realistic conditions, in particular, focusing on a Binomial quantum error correction code with loss as an error model for the quantum memories at the repeater stations. In addition and more specifically, we have proposed a promising implementation using microwave cavities that achieves all four necessary key steps: state engineering, syndrome measurement, error correction, and entanglement swapping. Our simulations of a two-segment quantum repeater allowed us to examine memory loss errors and the influence of the Binomial encoding. We found that both schemes with the Lower Binomial Code (LBC) and with the Higher Binomial Code (HBC) outperform the unencoded schemes for the same coherence times of the quantum memories. The HBC, even with lower coherence times, surpassed the performance of the unencoded protocols with higher coherence times. Moreover, we observed that multiple-error correction (MEC) provides a better secret key fraction (SKF) than single-error correction (SEC). We considered two different memory interface efficiencies, η_m , and found that the SKR trends are similar for the encoded and the unencoded cases. Our methods and results offer valuable guidance for optimizing repeater protocols in upcoming experiments.

As a next step, it is interesting to analyze multi-segment repeater systems and networks. There will be an optimal number of times recovery should be performed, as implementing error correction multiple times can also induce new errors. Exploring Binomial-code error correction in the context of third-generation quantum repeaters is a possible, promising direction as well. In this context, it would be useful to investigate state engineering in the optical domain and consider improving the 50% bound for logical Bell measurements for entanglement swapping. A rigorous rate analysis in the context of η_m would also be interesting to pursue. In summary, our findings demonstrate the promise of Binomial-code quantum error correction in advancing quantum repeater protocols and suggest important directions for future work.

ACKNOWLEDGMENTS

S.C. thanks Simon Reiß and Evgeny Shchukin for useful discussions. We acknowledge support from the Deutsche Forschungsgemeinschaft (DFG, German Research Foundation)—Project-ID 429529648—TRR 306 QuCoLiMa (“Quantum Cooperativity of Light and Matter”). S.C., F.S., and P.v.L. acknowledge funding from the Bundesministerium für Bildung und Forschung (BMBF) under the projects QR.X/QR.N, PhotonQ, and QuKuK. S.S. and S.V.K. acknowledge funding from the Bundesministerium für Bildung und Forschung (BMBF) under the project QECHQS (Grant No. 16KIS1590K).

Appendix A: Logical linear-optics Bell measurements

In this appendix, we show that a 50% success rate in entanglement swapping/Bell-state measurement (BSM) using linear optics can be achieved for lower-order Binomial codes when there is no loss on the codewords. This means, in our repeater scheme, we have to assume that a recovery operation is performed before the entanglement swapping takes place such that all states are mapped back onto the original codespace.

The BSM requires to distinguish the logical two-qubit states given in Eq. (19). Now first notice that $|\bar{\Phi}^\pm\rangle$ only contain Fock states of 0, 4, and 8 photons, whereas $|\bar{\Psi}^\pm\rangle$ only have terms with 2 and 6 photons. We will apply a beam splitter that preserves the total photon number in each term and so accepting only 2 or 6 photons at the detectors will unambiguously identify the two Bell states $|\bar{\Psi}^\pm\rangle$. In order to discriminate among these two states, we have to examine the possible number patterns of the two-mode state at the output of the beam splitter operation, \hat{BS} . A 50/50 beam splitter transforms $|\bar{\Psi}^\pm\rangle$ as

$$\begin{aligned} |\bar{\Psi}^\pm\rangle &= \frac{|\bar{0}\bar{1}\rangle \pm |\bar{1}\bar{0}\rangle}{\sqrt{2}} \\ &= \frac{1}{\sqrt{2}} \left(\frac{|0\rangle + |4\rangle}{\sqrt{2}} |2\rangle \pm |2\rangle \frac{|0\rangle + |4\rangle}{\sqrt{2}} \right) \\ &= \frac{1}{2} (|02\rangle \pm |20\rangle + |42\rangle \pm |24\rangle) \\ &\rightarrow \begin{cases} \frac{1}{2} [|20\rangle + |02\rangle + \hat{BS}(|42\rangle + |24\rangle)] \\ \frac{1}{2} [\sqrt{2}|11\rangle + \hat{BS}(|42\rangle - |24\rangle)] \end{cases} \end{aligned} \quad (\text{A1})$$

Here we have used $\hat{BS}|20\rangle = \frac{1}{2}(|20\rangle + |02\rangle) + \frac{1}{\sqrt{2}}|11\rangle$ and $\hat{BS}|02\rangle = \frac{1}{2}(|20\rangle + |02\rangle) - \frac{1}{\sqrt{2}}|11\rangle$ which means that $\frac{1}{\sqrt{2}}(|20\rangle + |02\rangle)$ remains invariant under the beam splitter transformation, while $\frac{1}{\sqrt{2}}(|20\rangle - |02\rangle)$ becomes $|11\rangle$ (like an inverse Hong-Ou-Mandel effect). Thus, click patterns ‘11’ and ‘20/02’ unambiguously identify the states $|\bar{\Psi}^-$ and $|\bar{\Psi}^+$, respectively. It then remains to be shown that also the patterns that originate from $\hat{BS}(|42\rangle \pm |24\rangle)$ are in one-to-one correspondence to the two different Bell states. This can easily be inferred from the following beam splitter transformations:

$$\begin{aligned} \hat{BS}|24\rangle &= \frac{1}{8} \left[\sqrt{15}|06\rangle + \sqrt{10}|15\rangle \right. \\ &\quad \left. - |24\rangle - 2\sqrt{3}|33\rangle - |42\rangle \right. \\ &\quad \left. + \sqrt{10}|51\rangle + \sqrt{15}|60\rangle \right], \\ \hat{BS}|42\rangle &= \frac{1}{8} \left[\sqrt{15}|06\rangle - \sqrt{10}|15\rangle \right. \\ &\quad \left. - |24\rangle + 2\sqrt{3}|33\rangle - |42\rangle \right. \\ &\quad \left. - \sqrt{10}|51\rangle + \sqrt{15}|60\rangle \right]. \end{aligned} \quad (\text{A2})$$

From the above equations, it is clear that the states BS ($|42\rangle \pm |24\rangle$) produce the unique click patterns ‘06’, ‘24’, ‘42’, ‘60’ and ‘15’, ‘33’, ‘51’, respectively. As a consequence, this proves that half of the Bell states can always be unambiguously identified, thus leading to a 50% BSM efficiency.

Appendix B: Recovery operators

The no-loss recovery operator for the LBC in the linear loss order, as given in the main text by Eq. (11), can be equivalently written as (using the notation from Ref. [21])

$$\begin{aligned} \mathcal{R}_0 = & (\sin(\log(1-\gamma)))(|E_0^0\rangle \langle \bar{0}| - |\bar{0}\rangle \langle E_0^0|) \\ & + (\cos(\log(1-\gamma)))(|\bar{0}\rangle \langle \bar{0}| + |E_0^0\rangle \langle E_0^0|) \\ & + |\bar{1}\rangle \langle \bar{1}|, \end{aligned} \quad (\text{B1})$$

where $|E_0^0\rangle = (|0\rangle - |4\rangle)/\sqrt{2}$. Note that $\mathcal{R}_0 = \text{id}$ when $\gamma = 0$.

The no-loss recovery operator for the HBC is given by [21]

$$\begin{aligned} \mathcal{R}_0 = & \sum_{\sigma} \sqrt{1 - \frac{|\langle \hat{B}_0 \rangle|^2}{\beta_0}} (|W_{\sigma}\rangle \langle B_{\sigma}^0| - |B_{\sigma}^0\rangle \langle W_{\sigma}|) \\ & + \frac{\langle \hat{B}_0 \rangle}{\sqrt{\beta_0}} (|W_{\sigma}\rangle \langle W_{\sigma}| + |B_{\sigma}^0\rangle \langle B_{\sigma}^0|), \end{aligned} \quad (\text{B2})$$

where $|W_{\sigma}\rangle$ is the codeword,

$$\beta_0 = \langle W_{\sigma} | \hat{B}_0^{\dagger} \hat{B}_0 | W_{\sigma} \rangle, \quad (\text{B3})$$

$\hat{B}_0 = 1 - \log(1-\gamma)\hat{n}/2 + (\log(1-\gamma))^2\hat{n}^2/8$, and

$$|B_{\sigma}^0\rangle = \frac{(1 - |W_{\sigma}\rangle \langle W_{\sigma}|) \hat{B}_0 |W_{\sigma}\rangle}{\sqrt{\beta_0 - |\langle \hat{B}_0 \rangle|^2}}. \quad (\text{B4})$$

The one-loss recovery operator for the HBC is given by

$$\begin{aligned} \mathcal{R}_1 = & |\bar{0}\rangle \langle 5| - |5\rangle \langle \bar{0}| \\ & + \frac{1}{\sqrt{2}} |\bar{1}\rangle (\langle 2| + \langle 8|) - \frac{1}{\sqrt{2}} (|2\rangle + |8\rangle) \langle \bar{1}|. \end{aligned} \quad (\text{B5})$$

The two-loss recovery operator for the HBC is given by

$$\begin{aligned} \mathcal{R}_2 = & |\bar{0}\rangle \langle 4| - |4\rangle \langle \bar{0}| + |\bar{1}\rangle \left(\frac{1}{\sqrt{5}} \langle 1| + \frac{2}{\sqrt{5}} \langle 7| \right) \\ & - \left(\frac{1}{\sqrt{5}} |1\rangle + \frac{2}{\sqrt{5}} |7\rangle \right) \langle \bar{1}|. \end{aligned} \quad (\text{B6})$$

Appendix C: Multiple rounds of error correction

Here, we consider a scheme with multiple rounds of quantum error correction where we perform one round thereof after a fixed number of time steps t_k . Thus, we calculate the concatenation of the loss channel after l time states followed by the recovery operation, which we will refer to as C^l , for $l \in \{1, \dots, t_k\}$. As an example let us consider that one quantum memory needs to wait for 100 time steps until entanglement is also distributed in the other segment and we choose t_k to be 30. The resulting final noise channel is then given by $C^{10}(C^{30}(C^{30}(\cdot)))$. Here we can see that we have to concatenate many channels. We do this concatenation by mapping the channel onto a vector of coefficients and the vector of coefficients after the concatenation can be obtained by multiplying the old vector of coefficients with a matrix. The mapping works as follows: For simplicity, we consider a qubit channel, i.e., we will project C^l onto a map that acts within the logical qubit space and a map that maps from the logical qubit space outside the codespace. Thus, we neglect parts mapping from outside the code space onto the codespace. Each single-qubit channel \mathcal{C} can be written in Kraus-operator representation $\sum_{j=1}^4 \sqrt{p_j} \hat{U}_j \cdot \hat{U}_j^{\dagger} \sqrt{p_j}$, where p_j are probabilities and \hat{U}_j are unitary operators. Pauli operators form an orthogonal basis with respect to the Frobenius inner product $\langle a, \hat{B} \rangle = \text{Tr}(a^{\dagger} \hat{B})$. Thus, we can write $\hat{U}_j = \alpha_{j0}1 + \alpha_{j1}\sigma_1 + \alpha_{j2}\sigma_2 + \alpha_{j3}\sigma_3$. We can simplify the next expressions by defining $\sigma_0=1$ and $\mathcal{N} = \sum_{j=0}^3 \sum_{k,l} p_j \alpha_{jk} \sigma_k \cdot \sigma_l \alpha_{jl}^* = \sum_{k,l} p_{kl} \sigma_k \cdot \sigma_l$, where $p_{kl} = \sum_{j=0}^3 p_j \alpha_{jk} \alpha_{jl}^*$. The coefficients p_{kl} then contain the complete information of the channel. When considering the concatenation of two channels one can find that the new channel is simply given by the product of a matrix defined by the outer channel and the vector of coefficients of the inner channel. Thus, the multiple concatenations of the same channel can be represented by a matrix product.

[1] H. J. Kimble, The quantum internet, *Nature* **453**, 1023–1030 (2008).
 [2] G. B. C. H. Bennett, Quantum cryptography: Public key distribution and coin tossing, *IEEE* **175**, 8 (1984).
 [3] A. K. Ekert, Quantum cryptography based on bell’s theorem, *Phys. Rev. Lett.* **67**, 661 (1991).

[4] M. Caleffi, M. Amoretti, D. Ferrari, J. Illiano, A. Manzalini, and A. S. Cacciapuoti, Distributed quantum computing: A survey, *Computer Networks* **254**, 110672 (2024).
 [5] J. F. Fitzsimons, Private quantum computation: an introduction to blind quantum computing and related pro-

- ocols, *npj Quantum Information* **3**, 10.1038/s41534-017-0025-3 (2017).
- [6] H.-J. Briegel, W. Dür, J. I. Cirac, and P. Zoller, Quantum repeaters: The role of imperfect local operations in quantum communication, *Phys. Rev. Lett.* **81**, 5932 (1998).
- [7] S. Muralidharan, L. Li, J. Kim, N. Lütkenhaus, M. D. Lukin, and L. Jiang, Optimal architectures for long distance quantum communication, *Scientific Reports* **6** (2016).
- [8] L.-M. Duan, M. D. Lukin, J. I. Cirac, and P. Zoller, Long-distance quantum communication with atomic ensembles and linear optics, *Nature* **414**, 413 (2001).
- [9] M. Pompili, S. L. N. Hermans, S. Baier, H. K. C. Beukers, P. C. Humphreys, R. N. Schouten, R. F. L. Vermeulen, M. J. Tiggeleman, L. dos Santos Martins, B. Dirkse, S. Wehner, and R. Hanson, Realization of a multinode quantum network of remote solid-state qubits, *Science* **372**, 259 (2021).
- [10] Y. Jing and M. Razavi, Quantum repeaters with encoding on nitrogen-vacancy-center platforms, *Phys. Rev. Appl.* **18**, 024041 (2022).
- [11] P. Loock, W. Alt, C. Becher, O. Benson, H. Boche, C. Deppe, J. Eschner, S. Höfling, D. Meschede, P. Michler, F. Schmidt, and H. Weinfurter, Extending quantum links: Modules for fiber- and memory-based quantum repeaters, *Advanced Quantum Technologies* **3**, 1900141 (2020).
- [12] R. Laurenza, N. Walk, J. Eisert, and S. Pirandola, Rate limits in quantum networks with lossy repeaters, *Phys. Rev. Res.* **4**, 023158 (2022).
- [13] L. Kamin, E. Shchukin, F. Schmidt, and P. van Loock, Exact rate analysis for quantum repeaters with imperfect memories and entanglement swapping as soon as possible, *Phys. Rev. Res.* **5**, 023086 (2023).
- [14] M. Razavi, M. Piani, and N. Lütkenhaus, Quantum repeaters with imperfect memories: Cost and scalability, *Phys. Rev. A* **80**, 032301 (2009).
- [15] S. Santra, L. Jiang, and V. S. Malinovsky, Quantum repeater architecture with hierarchically optimized memory buffer times, *Quantum Science and Technology* **4**, 025010 (2019).
- [16] S. D. Reiß and P. van Loock, Deep reinforcement learning for key distribution based on quantum repeaters, *Phys. Rev. A* **108**, 012406 (2023).
- [17] A. Romanova and P. van Loock, Memory-corrected quantum repeaters with adaptive syndrome identification, *Phys. Rev. Res.* **7**, 013117 (2025).
- [18] S. Haldar, P. J. Barge, S. Khatri, and H. Lee, Fast and reliable entanglement distribution with quantum repeaters: Principles for improving protocols using reinforcement learning, *Phys. Rev. Appl.* **21**, 024041 (2024).
- [19] K. Goodenough, T. Coopmans, and D. Towsley, On noise in swap asap repeater chains: exact analytics, distributions and tight approximations (2024), arXiv:2404.07146 [quant-ph].
- [20] N. Sangouard, C. Simon, H. de Riedmatten, and N. Gisin, Quantum repeaters based on atomic ensembles and linear optics, *Rev. Mod. Phys.* **83**, 33 (2011).
- [21] M. H. Michael, M. Silveri, R. T. Brierley, V. V. Albert, J. Salmilehto, L. Jiang, and S. M. Girvin, New class of quantum error-correcting codes for a bosonic mode, *Phys. Rev. X* **6**, 031006 (2016).
- [22] Z. Leghtas, G. Kirchmair, B. Vlastakis, R. J. Schoelkopf, M. H. Devoret, and M. Mirrahimi, Hardware-efficient autonomous quantum memory protection, *Phys. Rev. Lett.* **111**, 120501 (2013).
- [23] M. Mirrahimi, Z. Leghtas, V. V. Albert, S. Touzard, R. J. Schoelkopf, L. Jiang, and M. H. Devoret, Dynamically protected cat-qubits: a new paradigm for universal quantum computation, *New Journal of Physics* **16**, 045014 (2014).
- [24] D. Gottesman, A. Kitaev, and J. Preskill, Encoding a qubit in an oscillator, *Phys. Rev. A* **64**, 012310 (2001).
- [25] S. Häussler and P. van Loock, Quantum repeaters based on stationary gottesman-kitaev-preskill qubits (2024), arXiv:2406.07158 [quant-ph].
- [26] X. Gu, A. F. Kockum, A. Miranowicz, Y. xi Liu, and F. Nori, Microwave photonics with superconducting quantum circuits, *Physics Reports* **718-719**, 1 (2017), microwave photonics with superconducting quantum circuits.
- [27] A. Blais, A. L. Grimsmo, S. M. Girvin, and A. Wallraff, Circuit quantum electrodynamics, *Rev. Mod. Phys.* **93**, 025005 (2021).
- [28] S. Kuhr, S. Gleyzes, C. Guerlin, J. Bernu, U. B. Hoff, S. Deléglise, S. Osnaghi, M. Brune, J.-M. Raimond, S. Haroche, E. Jacques, P. Bosland, and B. Visentin, Ultrahigh finesse Fabry-Pérot superconducting resonator, *Applied Physics Letters* **90**, 164101 (2007).
- [29] A. Eickbusch, V. Sivak, A. Z. Ding, S. S. Elder, S. R. Jha, J. Venkatraman, B. Royer, S. M. Girvin, R. J. Schoelkopf, and M. H. Devoret, Fast universal control of an oscillator with weak dispersive coupling to a qubit, *Nature Physics* **18**, 1464 (2022).
- [30] P. Li and P. van Loock, Memoryless quantum repeaters based on cavity-qed and coherent states, *Advanced Quantum Technologies* **6**, 10.1002/qute.202200151 (2023).
- [31] L. Hu, Y. Ma, W. Cai, X. Mu, Y. Xu, W. Wang, Y. Wu, H. Wang, Y. P. Song, C.-L. Zou, S. M. Girvin, L.-M. Duan, and L. Sun, Quantum error correction and universal gate set operation on a binomial bosonic logical qubit, *Nature Physics* **15**, 503 (2019).
- [32] R. W. Heeres, P. Reinhold, N. Ofek, L. Frunzio, L. Jiang, M. H. Devoret, and R. J. Schoelkopf, Implementing a universal gate set on a logical qubit encoded in an oscillator, *Nature Communications* **8**, 94 (2017).
- [33] V. V. Sivak, A. Eickbusch, B. Royer, S. Singh, I. Tsioutsios, S. Ganjam, A. Miano, B. L. Brock, A. Z. Ding, L. Frunzio, S. M. Girvin, R. J. Schoelkopf, and M. H. Devoret, Real-time quantum error correction beyond break-even, *Nature* **616**, 50 (2023).
- [34] P. Li, J. Dias, W. J. Munro, P. van Loock, K. Nemoto, and N. Lo Piparo, Performance of rotation-symmetric bosonic codes in a quantum repeater network, *Advanced Quantum Technologies* **7**, 10.1002/qute.202300252 (2024).
- [35] J.-W. Pan, D. Bouwmeester, H. Weinfurter, and A. Zeilinger, Experimental entanglement swapping: Entangling photons that never interacted, *Phys. Rev. Lett.* **80**, 3891 (1998).
- [36] M. Żukowski, A. Zeilinger, M. A. Horne, and A. K. Ekert, “event-ready-detectors” bell experiment via entanglement swapping, *Phys. Rev. Lett.* **71**, 4287 (1993).
- [37] Y. Wu, J. Liu, and C. Simon, Near-term performance of quantum repeaters with imperfect ensemble-based quantum memories, *Phys. Rev. A* **101**, 042301 (2020).

- [38] M. A. Nielsen and I. L. Chuang, *Quantum Computation and Quantum Information: 10th Anniversary Edition* (Cambridge University Press, 2011).
- [39] H. P. Breuer and F. Petruccione, *The theory of open quantum systems* (Oxford University Press, 2002).
- [40] S. Sharma, V. S. V. Bittencourt, and S. V. Kusminskiy, Protocol for generating an arbitrary quantum state of the magnetization in cavity magnonics, *Journal of Physics: Materials* **5**, 034006 (2022).
- [41] N. Lauk, N. Sinclair, S. Barzanjeh, J. P. Covey, M. Saffman, M. Spiropulu, and C. Simon, Perspectives on quantum transduction, *Quantum Science and Technology* **5**, 020501 (2020).
- [42] R. W. Andrews, R. W. Peterson, T. P. Purdy, K. Cicak, R. W. Simmonds, C. A. Regal, and K. W. Lehnert, Bidirectional and efficient conversion between microwave and optical light, *Nature Physics* **10**, 321 (2014).
- [43] R. Sahu, L. Qiu, W. Hease, G. Arnold, Y. Minoguchi, P. Rabl, and J. M. Fink, Entangling microwaves with light, *Science* **380**, 718 (2023).
- [44] L. Sun, A. Petrenko, Z. Leghtas, B. Vlastakis, G. Kirchmair, K. M. Sliwa, A. Narla, M. Hatridge, S. Shankar, J. Blumoff, L. Frunzio, M. Mirrahimi, M. H. Devoret, and R. J. Schoelkopf, Tracking photon jumps with repeated quantum non-demolition parity measurements, *Nature* **511**, 444 (2014).
- [45] F. Okamoto, M. Endo, M. Matsuyama, Y. Ishizuka, Y. Liu, R. Sakakibara, Y. Hashimoto, J.-i. Yoshikawa, P. van Loock, and A. Furusawa, Phase locking between two all-optical quantum memories, *Phys. Rev. Lett.* **125**, 260508 (2020).
- [46] Y. Hashimoto, T. Toyama, J.-i. Yoshikawa, K. Makino, F. Okamoto, R. Sakakibara, S. Takeda, P. van Loock, and A. Furusawa, All-optical storage of phase-sensitive quantum states of light, *Phys. Rev. Lett.* **123**, 113603 (2019).
- [47] J.-i. Yoshikawa, K. Makino, S. Kurata, P. van Loock, and A. Furusawa, Creation, storage, and on-demand release of optical quantum states with a negative wigner function, *Phys. Rev. X* **3**, 041028 (2013).
- [48] Z. Aqua, M. S. Kim, and B. Dayan, Generation of optical fock and w states with single-atom-based bright quantum scissors, *Photon. Res.* **7**, A45 (2019).
- [49] N. Rivera, J. Sloan, Y. Salamin, J. D. Joannopoulos, and M. Soljačić, Creating large fock states and massively squeezed states in optics using systems with nonlinear bound states in the continuum, *Proceedings of the National Academy of Sciences* **120**, e2219208120 (2023).
- [50] Z. Leghtas, G. Kirchmair, B. Vlastakis, M. H. Devoret, R. J. Schoelkopf, and M. Mirrahimi, Deterministic protocol for mapping a qubit to coherent state superpositions in a cavity, *Phys. Rev. A* **87**, 042315 (2013).
- [51] K. Fukui, R. N. Alexander, and P. van Loock, All-optical long-distance quantum communication with gottesman-kitaev-preskill qubits, *Phys. Rev. Res.* **3**, 033118 (2021).
- [52] F. Rozpędek, K. Noh, Q. Xu, S. Guha, and L. Jiang, Quantum repeaters based on concatenated bosonic and discrete-variable quantum codes, *npj Quantum Information* **7**, 102 (2021).
- [53] F. Rozpędek, K. P. Seshadreesan, P. Polakos, L. Jiang, and S. Guha, All-photonic gottesman-kitaev-preskill-qubit repeater using analog-information-assisted multiplexed entanglement ranking, *Phys. Rev. Res.* **5**, 043056 (2023).
- [54] F. Schmidt, D. Miller, and P. van Loock, Error-corrected quantum repeaters with gottesman-kitaev-preskill qudits, *Phys. Rev. A* **109**, 042427 (2024).
- [55] N. Sangouard, C. Simon, H. de Riedmatten, and N. Gisin, Quantum repeaters based on atomic ensembles and linear optics, *Rev. Mod. Phys.* **83**, 33 (2011).
- [56] E. Shchukin, F. Schmidt, and P. van Loock, Waiting time in quantum repeaters with probabilistic entanglement swapping, *Phys. Rev. A* **100**, 032322 (2019).
- [57] M. Reitz, C. Sommer, and C. Genes, Cooperative quantum phenomena in light-matter platforms, *PRX Quantum* **3**, 010201 (2022).
- [58] F. Wulschner, J. Goetz, F. R. Koessel, E. Hoffmann, A. Baust, P. Eder, M. Fischer, M. Haeberlein, M. J. Schwarz, M. Pernpeintner, E. Xie, L. Zhong, C. W. Zollitsch, B. Peropadre, J.-J. Garcia Ripoll, E. Solano, K. G. Fedorov, E. P. Menzel, F. Deppe, A. Marx, and R. Gross, Tunable coupling of transmission-line microwave resonators mediated by an rf squid, *EPJ Quantum Technology* **3**, 10 (2016).
- [59] S. Pirandola, R. Laurenza, C. Ottaviani, and L. Banchi, Fundamental limits of repeaterless quantum communications, *Nature Communications* **8**, 10.1038/ncomms15043 (2017).
- [60] Ángel Rivas and S. F. Huelga, *Open Quantum Systems: An Introduction* (Springer Berlin, Heidelberg, 2012).